Marine Geology 279 (2011) 128–140

Contents lists available at ScienceDirect

Marine Geology

journal homepage: www.elsevier.com/locate/margeo

Geochemistry and stable isotope constraints on high-temperature activity from sediment cores of the Saldanha hydrothermal field

Á.S. Dias [a,*], G.L. Früh-Green [b], S.M. Bernasconi [c], F.J.A.S. Barriga [a] and Seahma cruise team, Charles Darwin 167 cruise team

[a] CREMINER, Department of Geology, University of Lisbon, FCUL Edificio C6, Piso4, Campo Grande, Lisbon 1749-016, Portugal
[b] Institute of Geochemistry and Petrology, ETH, Clausiusstr. 25, Zurich CH-8092, Switzerland
[c] Geological Institute, ETH, Sonneggstr. 5, Zurich CH-8092, Switzerland

ARTICLE INFO

Article history:
Received 13 May 2009
Received in revised form 23 June 2010
Accepted 19 October 2010
Available online 27 October 2010

Communicated by D.J.W. Piper

Keywords:
Saldanha hydrothermal site
stable isotopes
hydrothermal calcite
serpentinization heat source

ABSTRACT

The Saldanha hydrothermal field is hosted atop a mafic–ultramafic seamount, located at a non-transform offset on the Mid-Atlantic Ridge. Previous observations revealed a field where transparent low-temperature fluids discharge through centimeter-sized vents without the formation of chimney structures. We present geochemical and stable isotope (O and C) analyses from sediment samples collected at this field, both at and far from the vent area. Most sediments, including some directly adjacent to orifice vents, are pelagic oozes with only a weak hydrothermal overprinting. Hydrothermal precipitates are characterized by Fe–Mn oxyhydroxides and a minor amount of Cu–Zn sulphide minerals. However, one of the cores (SCD7) collected at the vent area shows a much stronger hydrothermal signature. This core is composed of a matrix of serpentine + talc ± chlorite with high porosity, where calcite + chalcopyrite + sphalerite/wurtzite ± pyrite–pyrrhotite were precipitated. In this core, metal enrichments, REE patterns, and the oxygen and carbon isotope composition of calcites indicate that mineralization must have occurred in the subsurface by high-temperature fluids, with minor mixing with seawater and with a significant magmatic contribution. Thus, while most samples confirm previous findings indicating that Saldanha hydrothermal fluid discharge is mainly diffuse and of low temperature, data from core SCD7 suggest that areas of high-temperature hydrothermal activity also occur, where temperatures of the fluids could reach >260 °C and maximum temperatures of 330 °C. We suggest that fluids can flow through faults at the top of the mount and discharge in a more focused way through vent orifices, producing intense hydrothermal alteration of the sediments. At these locations complex hydrothermal processes occur, including reactions of the hydrothermal fluids with mafic and ultramafic rocks and magma degassing, as suggested by the carbon isotope composition of hydrothermal calcites. The high temperature of the fluid inferred from the geochemistry of the hydrothermal minerals requires a significant heat input to the system, suggesting an additional magmatic heat source to the already proposed exothermic serpentinization reactions.

1. Introduction

Until recently, submarine hydrothermal activity was thought to be associated primarily with Mid-Ocean Ridges (MOR) and driven by the cooling of basaltic or gabbroic rocks. However, the discovery of hydrothermal activity associated with exposed serpentinized peridotites has added a new perspective to our understanding of seafloor hydrothermal processes. The focus on these ultramafic-hosted hydrothermal systems has increased, i.e., in relation to their heat sources (e.g., Allen and Seyfried, 2004; Bach et al., 2002; Früh-Green et al., 2003; Fyfe, 1974; Kelley et al., 2001, 2005; Lowell and Rona, 2002; Marques et al., 2007; Schroeder et al., 2002), fluid compositions (e.g., Allen and Seyfried, 2003; Charlou et al., 2002; Douville et al., 2002; Proskurowski et al., 2006, 2008; Schmidt et al., 2007), oceanic lithosphere rheology and geophysical properties (e.g., Dyment et al., 1997; Escartin et al., 1997, 2003; Mevel, 2003), hydrothermal sediments and plume particles (e.g., Cave et al., 2002; Chavagnac et al., 2006; Dias and Barriga, 2006; Edmonds and German, 2004), and microbial processes (Alt et al., 1998; Brazelton et al., 2006; Holm and Charlou, 2001; Kelley et al., 2001, 2005; O'Brien et al., 1998; Perner et al., 2007).

The seafloor exposure of serpentinized peridotites is a common feature along slow spreading MOR and is especially associated with crustal thinning, with low or focused volcanic activity and with the development of extensional low angle faults (Cannat, 1993; Cannat et al., 1995; Dick et al., 2008; Escartin and Cannat, 1999; Escartín et al., 1997; Gràcia et al., 2000; Smith et al., 2006). The faulting network in

* Corresponding author.
E-mail addresses: agata.dias@fc.ul.pt (Á.S. Dias), frueh-green@erdw.ethz.ch (G.L. Früh-Green), stefano.bernasconi@erdw.ethz.ch (S.M. Bernasconi), f.barriga@fc.ul.pt (F.J.A.S. Barriga).

0025-3227/$ – see front matter © 2010 Elsevier B.V. All rights reserved.
doi:10.1016/j.margeo.2010.10.017

these environments allows deeper crustal seawater penetration promoting serpentinization through hydration reactions involving olivine and pyroxene (e.g., Janecky and Seyfried, 1986; Seyfried and Dibble, 1980; Seyfried et al., 2007; Wetzel and Shock, 2000).

Several active hydrothermal systems hosted in serpentinized ultramafic rocks have been discovered along the Mid-Atlantic Ridge (MAR). They comprise either high-temperature vent fields with major sulphide deposits, such as Rainbow at 36°14′N (Fouquet et al., 1997; German et al., 1996a) and Logatchev at 14°45′N (Bogdanov et al., 1997), or lower temperature fields, such as Lost City at 30°N (Früh-Green et al., 2003; Kelley et al., 2001, 2005) and Saldanha at 36°30′N (Barriga et al., 1998; Dias and Barriga, 2006).

In the high-temperature fields, the hot (up to 400 °C) vent fluids are enriched in metals and generate black smoker chimneys on the seafloor. The lower temperature (up to 90 °C) fields may form carbonate chimneys (e.g., Lost City) or vent orifices without chimney structures (e.g., Saldanha) (e.g., Barriga et al., 1998; Dias and Barriga, 2006; Früh-Green et al., 2003; Kelley et al., 2005). Studies on vent fluids derived from ultramafic-hosted systems show some differences in fluid chemistry, particularly in H_2 and CH_4 contents, when compared to basalt-hosted hydrothermal fields (Charlou et al., 2002; Douville et al., 2002; Kelley et al., 2001, 2005; Proskurowski et al., 2008; Schmidt et al., 2007). On a regional scale, the detection of high concentrations of CHB_{4B} and $HB_{2\ B}$ in the water column along slow and ultraslow spreading ridges, released as a result of peridotite–water reactions, indicate that hydrothermal systems are common in these environments (Charlou et al., 1993, 2002; German et al., 1996b; Seyfried et al., 2007).

The study of hydrothermal sediments is relevant for the understanding of hydrothermal processes because sediments, together with massive sulphides and hydrothermally altered rocks, are important records of hydrothermal activity (Hannington et al., 1995). Sediments associated with hydrothermal processes at MOR have been studied since the 1960s (Bonatti, 1981; Bonatti and Joensuu, 1966; Boström and Peterson, 1966). After these pioneer studies, a great number of geochemical and mineralogical investigations have been conducted on ocean ridge hydrothermal sediments. From these, it is now clear that hydrothermal sediments have a distinct mineralogical and geochemical signature in comparison to normal pelagic sediments (Boström and Peterson, 1969), in particular in the metal-rich precipitates (Mills and Elderfield, 1995a). Hydrothermal sediments can be formed by direct precipitation from hydrothermal fluids within the sediment; plume fallout or sulphide mass wasting and debris flow admixed with background pelagic, biogenic and terrigenous components (Mills and Elderfield, 1995b). The relative proportion of the hydrothermal component to the sediment background will determine the intensity of the geochemical and mineralogical hydrothermal signature.

The aim of this study is to investigate the variation of hydrothermal alteration in Saldanha sediments. Toward this goal we studied the variation in the mineralogy and geochemistry in 10 sediment cores. Additionally, stable isotope analyses of carbonates were used to constrain the temperature and composition of the hydrothermal fluids. Previous studies have shown that Saldanha sediments are pelagic foraminiferal oozes overprinted by a weak hydrothermal signature (Dias and Barriga, 2006) and most samples analysed in this work agree with this pattern. However, one core (SCD7) presents a much higher degree of hydrothermal alteration, unreported for Saldanha sediments, and thus our investigation focuses extensively on this core. These data provide an important basis for understanding the little-known Saldanha hydrothermal system and sheds new light on the hydrothermal processes and heat sources driving this site.

2. Geological setting

The Saldanha hydrothermal field is located at a non-transform offset (NTO5), between the FAMOUS and AMAR segments on the MAR (N36°34′; W33°26′). The NTO is characterized by a series of cross-cutting discontinuous faults with predominant E–W, NNW–SSE directions (Gràcia et al., 2000; Parson et al., 2000). A significant methane anomaly with low TDM (total dissolve manganese) levels was detected in the water column above this site during the FLAME, HEAT and FAZAR cruises (Bougault et al., 1998; Calvert and Price, 1970; Charlou et al., 1993, 1997; German et al., 1994, 1996b). This anomaly, together with rock sampling performed during the FLORES cruise (Fouquet et al., 1998), indicated the occurrence of serpentinized ultramafic rocks and was crucial in predicting hydrothermal activity related to serpentinization between the FAMOUS and AMAR segments.

The Saldanha field was discovered in 1998 during the Saldanha cruise (Barriga et al., 1998; Dias and Barriga, 2006). The site was revisited in 2001 during the Seahma cruise (Barriga et al., 2004) and in 2004 during the CD167 cruise (Sinha et al., 2006). It is a mafic–ultramafic-hosted hydrothermal field situated atop of one massif consisting of a 100 m high semi-circular dome that is slightly elongated in the NNE-SSW direction. Direct observations during submersible dives and detailed geophysical analyses of this structure have revealed that it is disturbed by NE–SW, E–W and WNW–ESE striking faults (Barriga et al., 2003; Miranda et al., 2003). *In situ* observations showed that hydrothermal activity takes place through diffuse discharge but more focused vents also exist. The vents are scarce and scattered on the ocean floor over an area of approximately 400 mP^{2P} and are characterized by the discharge of a clear fluid through centimeter-sized orifices without the growth of chimney-like or other structures. Fluid temperatures measured directly at the vent orifices with the ROV Victor during the 2001 Seahma mission were not higher than 9 °C. Because these vents lack a chimney structure, it was not possible to introduce the temperature probe inside the orifices and temperature was recorded some centimeters above the seafloor. Thus, venting temperatures remain unknown and are likely higher than those measured.

Sediments cover around 80% of the massif area and show variable thickness, from no sediment cover to almost 1 m thickness in the deeper parts around the flanks of the Saldanha dome. Bulk sediment analyses of the top sediment layers from cores of the 1998 Saldanha mission indicate the presence of a minor low-temperature hydrothermal component in the background foraminiferal ooze (Dias and Barriga, 2006). Saldanha basement lithologies are highly heterogeneous. Volcanic rocks are mainly dominant around the massif, but serpentinites, steatites (talc-bearing serpentinites) and meta-gabbros and basalts also occur (Fig. 1). Steatites and metagabbros are located essentially along the major faulting network of Saldanha, which may provide preferential conduits for hydrothermal fluid upflow (Dias et al., 2010). The occurrence of steatites are comparable to talc–amphibole–chlorite rich, detachment fault rocks resulting from focussed fluid flow and gabbro–seawater interaction that are typical of oceanic core complexes (Bach et al., 2004; Boschi et al., 2006a,b; Dick et al., 2008; Escartin et al., 2003).

3. Methods

Five sediment cores collected far from the vent area (SH86, SH92, SCD2, SCD3 and SCD8) and five at the vent area (SH49, SH63T, SH118T, SH119 and SCD7) during the Seahma I (Barriga et al., 2003) and CD167 (Dzhatieva et al., 2005; Sinha et al., 2005, 2006) missions in 2002 and 2004, respectively, were studied in this work (Fig. 1 and Table 1). Samples from the Seahma mission are identified with a SH prefix and CD167 samples with a SCD prefix. Cores SH63T, SH118T and SH119 were collected with the ROV at the vent orifices where temperature measurements were performed. Core SH49 was collected in the vent area but not in a vent orifice. Core SCD7 was collected from the vessel with a gravity corer at a location where it was known that the vents were highly concentrated, based on the mapping from

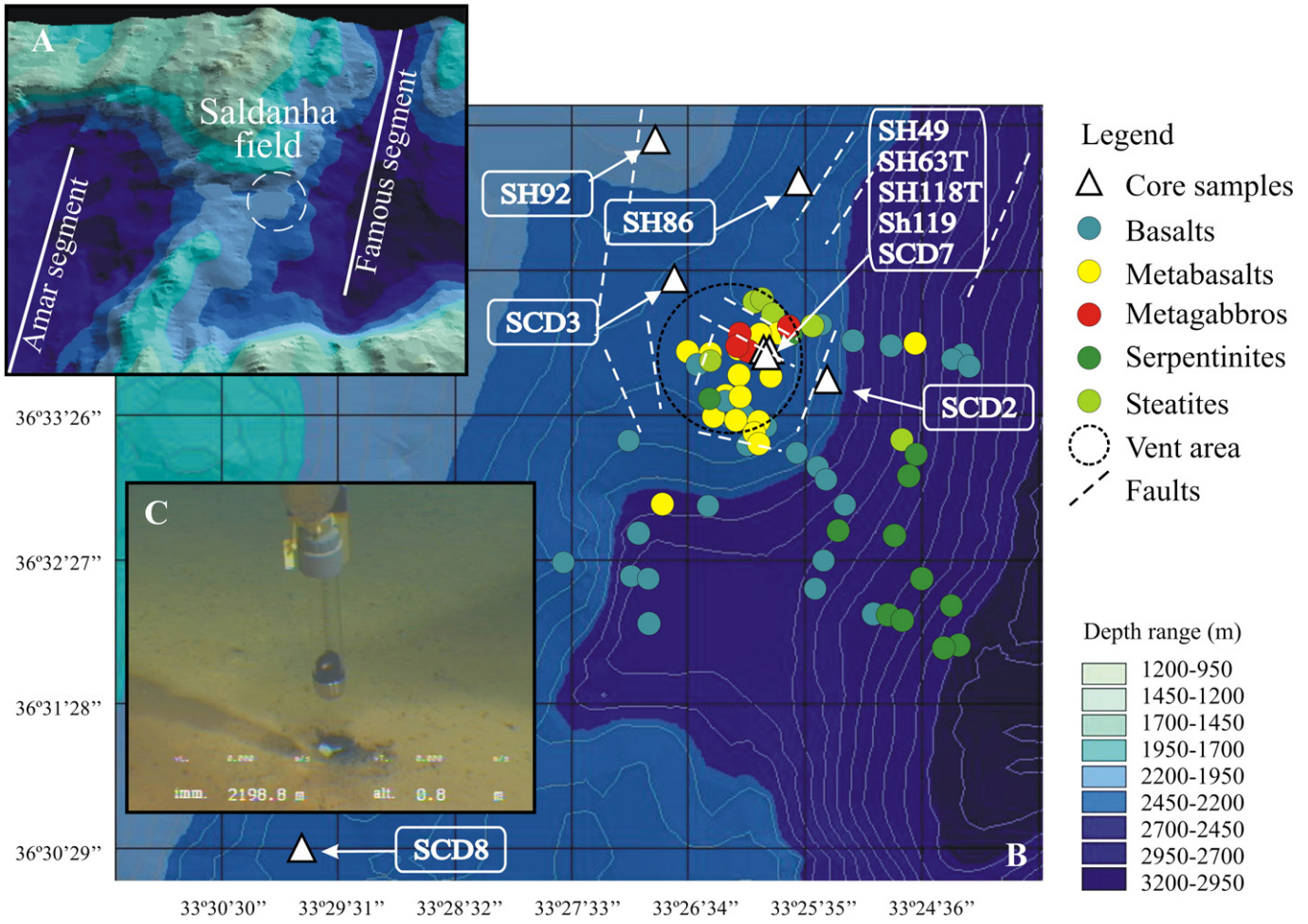

Fig. 1. (A) High-resolution bathymetry map of Saldanha hydrothermal field and surrounding area. Three-dimensional perspective generated from bathymetric mapping using ArcGis software digital elevation models (DEMs). (B) Saldanha map area with sample locations. Geological data (rock samples, hydrothermal vents area and main structures) are also projected. (C) Photo from a hydrothermal vent orifice before push-core sediment sampling.

the previous missions, but no direct observations of the field or vent temperature measurements were performed (see Table 1). Two samples (SH63T and SH118T) are labelled with a "T," indicating that downcore analyses were not possible and that the several core layers were mixed and averaged for analyses. At the SH63T sampling location sediment thickness and core recovery was low, which hindered detailed downcore analyses. The SH118T sample was capped by a Mn oxide crust and recovered with a spade after crust removal and thus the sediment arrived mixed at the surface.

After the cores were split, one half was archived and the other one was sliced in horizontal sections for petrographic and geochemical analyses. Sediment subsamples were dried and impregnated in epoxy resin to prepare polished sections for reflected and transmitted light microscopy. X-ray diffraction (XRD) analyses of bulk powdered sediments and of individual fragments were performed using a Philips PW 1710 diffractometer equipped with a Ni filter and CuKα radiation at 40 kV and 49 mA. A pure silicon sample holder (PW 1817/32) was used, which produces no interferences in the diffractograms and allows running small amounts of material.

Before geochemical analyses, rock fragments detected under a binocular microscope were removed. Major and minor elements and REE concentrations were determined by inductively coupled plasma optical emission spectrometry (ICP-OES), inductively coupled plasma mass spectrometry (ICP-MS) and instrumental neutron activation

Table 1
Characteristics of the sediment samples used in this study.

	Samples	Cruise/Sampling method	Core recovery (cm)	Measured T(°C) at the vent***	Depth (m)
Away from vents area	SH86	Seahma I, 2002 / ROV "push-corer"	12	–	3658
	SH92	Seahma I, 2002/ROV "push-corer"	12	–	2125
	SCD2	CD 167, 2004/Gravity core	164	–	2350
	SCD3	CD 167, 2004/Gravity core	150	–	2248
	SCD8	CD 167, 2004/Gravity core	91		- 2300
At the Vents area	SH49	Seahma I, 2002/ROV "push-corer"	11	–	2221
	SH63T*	Seahma I, 2002/ROV "push-corer"	-	7.8	2677
	SH118T*, **	Seahma I, 2002/ROV "spade"	-	9.0	2214
	SH119*	Seahma I, 2002/ROV "push-corer"	12	7.6	2213
	SCD7*	CD 167, 2004/Gravity core	27	–	2198

*Collected at an orifice vent; **sample covered by a Mn crust; ***measured a few centimeters above the vents.

analysis (INAA) (see Electronic Supplementary Data for further details). Geochemical analyses were carried out at Activation Laboratories, Ltd. (ACTLABS, Ontario, Canada) following standard procedures. The measurement precision for the major oxides was better than ±1%–2% and for the other elements better than 5%–10%. For REE the measurement precision was better than 5%.

Stable isotopes (O and C) were measured at the Geological Institute of the ETH in Zurich. Bulk carbonate and crystallized calcites were handpicked from the bulk sediment and analyzed for their O and C isotopic composition by reacting 100–200 μg of sample with 100% phosphoric acid using a Thermo Instruments Kiel IV carbonate preparation device. Isotope ratios were measured on a Thermo Instruments Delta V mass spectrometer and are reported as δ-values in per mil (‰) relative to Vienna Pee Dee Belemnite (VPDB) standard. The $\delta P^{18P}O$ values of calcite on the VPDB scale are converted to the Vienna Standard Mean Ocean Water standard (VSMOW) using the equation of Coplen et al. (1983): $\delta P^{18P}OB_{VSMOWB} = 1.03091\ \delta P^{18P}OB_{VPDBB} + 30.91$. Analytical precision based on repeated measurements of internal standards was better than 0.07‰ for both C and O.

Temperatures were calculated from O isotope data using the calcite-water fractionation curve of Friedman and O´Neil (1977).

4. Results and discussion

4.1. Sediment description

Petrographic observation revealed three main components in the Saldanha sediments: (1) a pelagic sediment fraction composed of biogenic carbonates and clays; (2) hydrothermal minerals; and (3) basement rock fragments. A qualitative description of the major components of each sample is given in Table 2 and representative photos are presented in Fig. 2. All cores were homogeneous from top to bottom, with the exception of SCD7, and thus a more detailed petrographic description is presented for this core.

The Saldanha sediments are mainly pelagic foraminiferal oozes with more than 80% carbonate and rare millimeter-sized rock fragments (Fig. 2A and 2B). The SH63T, SH118T and SH119 samples, collected directly at vent orifices, are characterized by Fe–Mn oxyhydroxides (todorokite and birnessite) with sporadic millimeter-sized grains of chalcopyrite, sphalerite and pyrite. Previous work has shown that the Fe–Mn oxyhydroxides have a clear hydrothermal origin (Dias and Barriga, 2005; Dias et al., 2005, 2010). These three samples contain rare rock fragments, characterized by altered ultramafic lithoclasts (steatites and serpentinites), while in the remaining cores, collected away from vent orifices, mafic rocks, when present, are the principal rock fragments. These compositional features are similar to those previously described by Dias and Barriga (2006) for Saldanha sediments.

4.1.1. Core SCD7

Core SCD7 yielded the most hydrothermally altered sediment (Fig. 2C). The first 5 cm contain fragments of metasomatized microgabbros, fine-grained ferromanganese oxyhydroxides (<5%) and sporadic foraminiferal tests with evident dissolution. Below this layer the sediment shows clear hydrothermal alteration, with variable detrital fragments and no biogenic constituents. The sediment has a high porosity and is formed, in general, by a matrix of serpentine and talc (Fig. 2D and E) and, in minor amounts, chlorite, with widespread Cu, Zn and Fe sulphides and calcite (Fig. 2F). Although rare below 5 cmbsf (centimeters below seafloor), variable millimeter-sized lithoclast fragments (<5 mm) of serpentinites, steatites and metagabbros/metabasalts, most of which showing deformation, are distributed throughout the core (Table 2). Chromite and magnetite occur sporadically as isolated grains or as components of the ultramafic lithoclasts.

The sulphide assemblage includes chalcopyrite and sphalerite/wurtzite with smaller amounts of pyrite and pyrrhotite (Fig. 2G–2J). These phases occur dominantly between 13 and 21 cmbsf and are deposited in situ as coarse-grained aggregates in open pore spaces and filling stockwork-like veins. Hexagonal euhedral crystals of sphalerite pseudomorphic after wurtzite are observed in the 5–7 cmbsf layer. The high concentrations of metals such as Cu and Zn implies that high-temperature fluids that interacted with gabbros/basaltic rocks were involved in sulphide precipitation, as ultramafic-derived fluids are metal-depleted (Schmidt et al., 2007). Metals are transported in acidic solutions, especially at high temperatures, which cause a large increase in metal complex stability (e.g., Vaughan and Craig, 1986). Sulphide precipitation, on the other hand, is favored by lower temperatures and more oxidizing conditions (Hannington et al., 1995; Large, 1992). Thus, the cooling of the ascending metal-rich

Table 2
Qualitative petrographic description of the major components from each core. Core SCD7 was highly heterogeneous downcore and thus a description of each layer is presented for this sample. The remaining cores were grouped according to their petrographic similarity.

Sediment cores	Talc/Serpentine	Calcite	Chlorite	Sulphide phases	Oxy-hydroxides	Oxides	Altered ultramafic rocks	Metassomatized mafic rocks	Microorganisms tests
SH49					–			x	xxx
SH86					–			x	xxx
SH92					–			x	xxx
SCD2					–			x	xxx
SCD3					–			x	xxx
SCD8					–			x	xxx
SH118T	x			x	xx		x		xxx
SH119	x			x	xx		x		xxx
SH63T	x			x	xx		x		xxx
SCD7 (cmbsf)									
top		x			x		x	xx	x
<5	xx	x		x	x		x	x	–
5–7	xx	xx	–	x			x	x	
7–8	xxx	xx	–	x			x	-	
9–10	xxx	xx	–	x		-	x	-	
11–13	xxx	xx	–	x		-	x	-	
13–16	xxx	xxx	–	x		-	x	-	
16–17	xxx	xxx	–	xx		-	x	-	
17–19	xxx	xxx	–	xx		x	x	-	
19–21	xxx	xxx	–	xx		x	x	-	
22–23	xxx	xx	–	xx			x	-	
25–27	x	xx	–	x			x	-	

( ) absent; (–) sporadic; (x) rare; (xx) abundant; (xxx) very abundant.

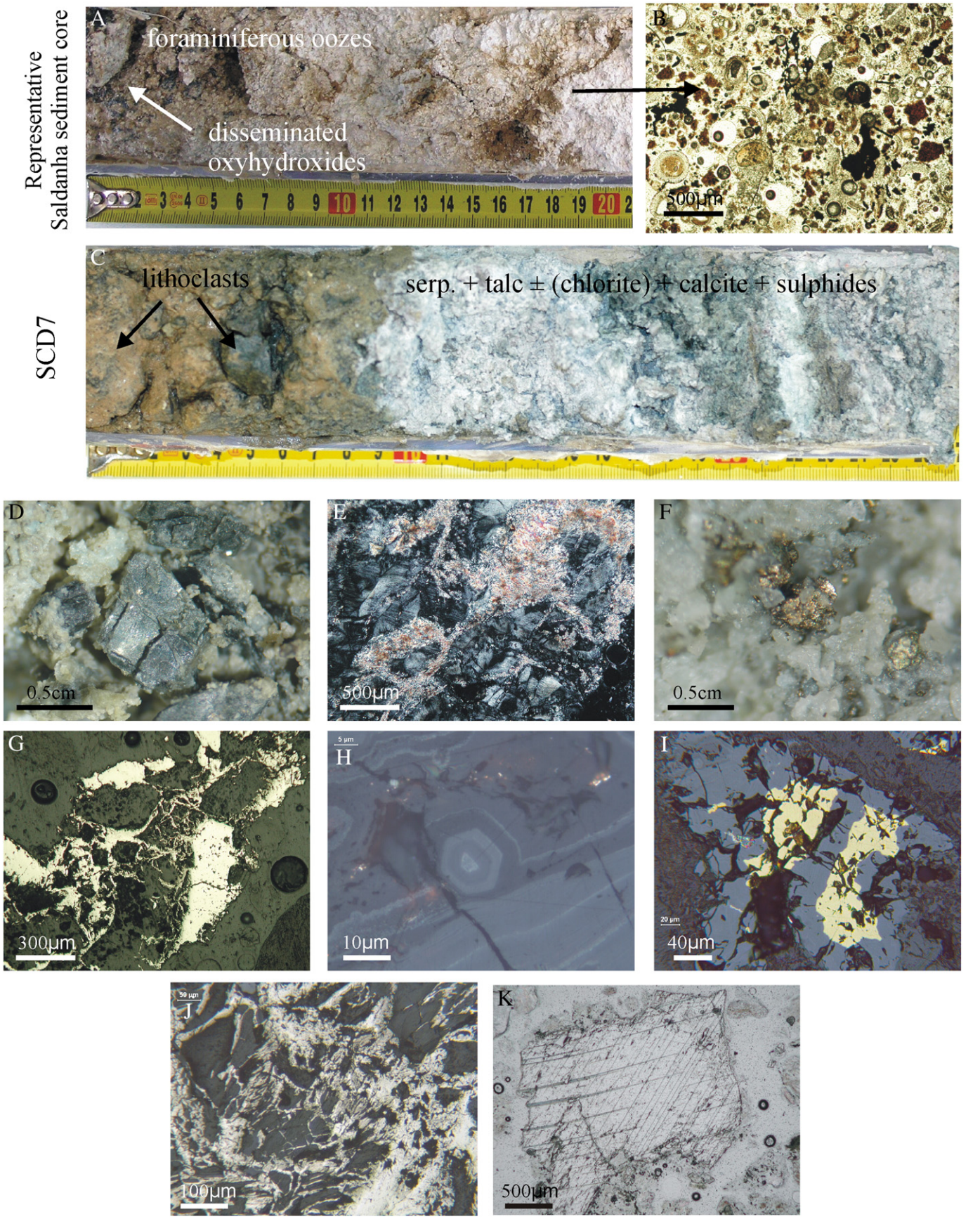

Fig. 2. (A) Macroscopic view of a whole-core longitudinal section of a representative Saldanha sample; (B) thin-section photomicrography (crossed-nicols) of foraminiferous oozes with oxyhydroxides; (C) macroscopic view of a whole-core longitudinal section of SCD7 sediment; (D and E) sediment background where serpentine and talk are visible; (F) hydrothermal calcite; (H) calcite + talc + serpentine; (G and J) stockwork-like veining filled with pyrite (reflected light); (H) sphalerite after wurtzite; (I) chalcopyrite surrounded by sphalerite; (K) white calcite. Photos d and f were taken with a binocular magnifier. Photos e and k were taken in a petrographic microscope with transmitted light and G–J with reflected light.

fluids and the increase in oxidation conditions closer to the surface causes their precipitation.

Large white calcite crystals up to 0.5 cm long were observed throughout the core (Fig. 2K), particularly between 13 and 21 cmbsf. Calcite occurs in association with sulphides. The presence of sulphide crystals on the calcite crystals indicate that calcite precipitated in situ before or at the same time as sulphides. Hydrothermal calcite precipitation has been described in many hydrothermal ore deposits (e.g., Moller et al., 1979, 1984, 1991; Zheng, 1990; Zheng and Hoefs, 1993) and is mainly controlled by changes in pH and temperature (Faure, 1986). In Saldanha, the increase in pH of hydrothermal fluids during mixing with seawater might by itself be sufficient for calcite precipitation. The Ca is most probably derived from the interaction between hydrothermal fluid and the carbonate sediments and from mixing with seawater. The underlying lithologies (peridotites and mafic rocks) may also contribute Ca to the hydrothermal fluids. Clinopyroxene breakdown during the serpentinization of peridotites can add Ca to the fluids, especially at temperatures higher than 250 °C (Allen and Seyfried, 2004). However, at Saldanha, the basement rocks are harzburgites with negligible clinopyroxene content (Ribeiro da Costa, 2005), implying that they are not the main source of Ca to form the large amount of calcite in the SCD7 sediment core. A magmatic Ca source is also possible, if Ca was mobilized from gabbros during fluid–rock interaction (e.g., Seyfried et al., 1988).

4.2. Geochemical composition of sediments and principal component analysis

4.2.1. Major and trace elements

Chemical compositions determined from bulk sediment analyses are given in the Electronic Supplementary Data. Two separate principal component analyses (PCA) were conducted, one using major element and another using trace element data. The PCAs generated two orthogonal vectors (PC1 and PC2), which together explain 91% of the variance in the major (Fig. 3A) and 85% of the variance in the trace elements (Fig. 3B).

With the exception of core SCD7 and samples collected directly at the vents, the chemistry of the Saldanha sediments is similar to an average pelagic foraminiferal ooze (e.g. Ben Othman et al., 1989; Plank and Langmuir, 1998; Van der Flier-Keller, 1991). For the major oxides, PC1 accounts for 71% of the variance in the data set and the higher positive load of this axis is given by the concentration of CaO. With the

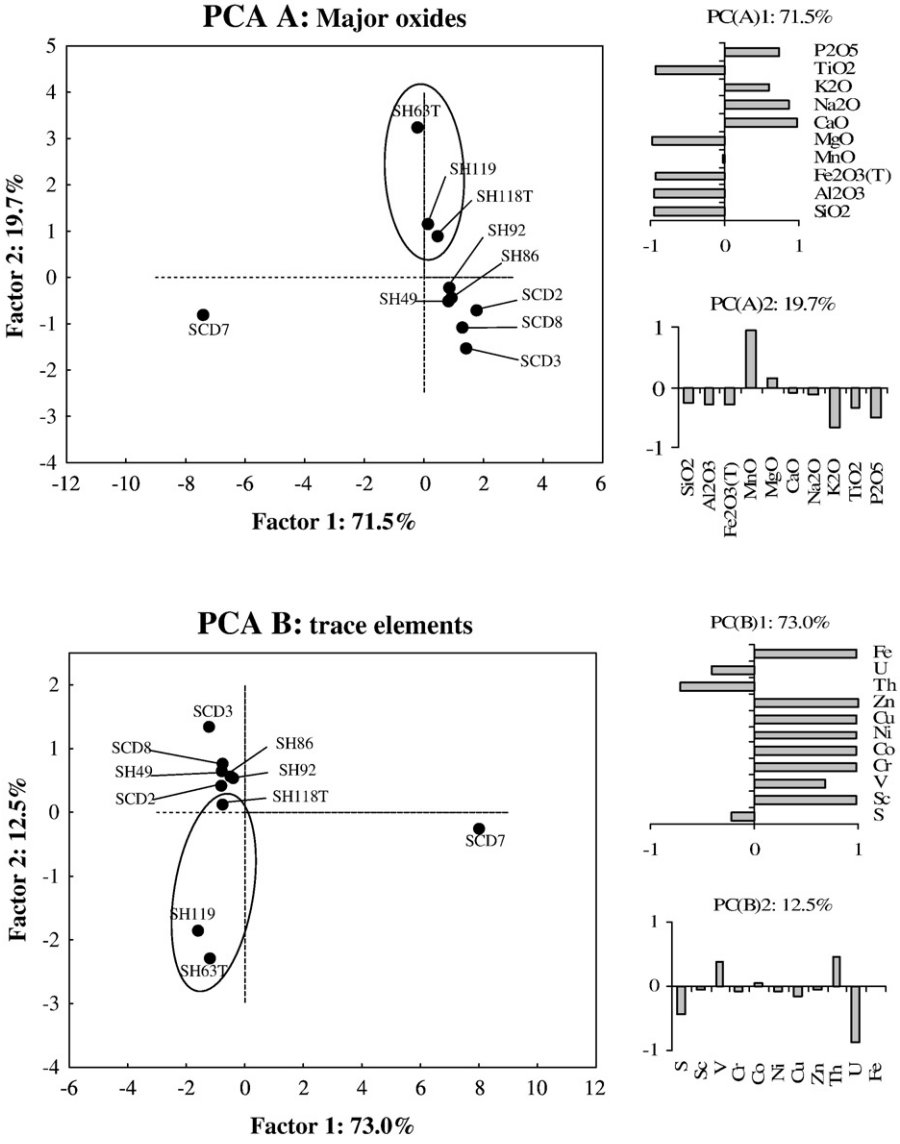

Fig. 3. PCA (Principal Component Analysis) plot of PC1 versus PC2 scores for major oxides (A) and trace (B) elements. For each sediment core, the average concentration in major oxides or trace elements was used in the PCA analyses. The PC1 and PC2 scores for each major oxide and trace element are given in the inset graphs. Samples collected directly at the vent orifices during ROV dives are marked with a circle.

exception of sample SCD7, CaO is the major oxide in all remaining samples. Other oxides are below 4% and are essentially incorporated into clays. The high concentration of Ca (33.9 ± 2.2 %) and C (10.4 ± 0.7%) and their positive correlation ($r = 0.94$, $N = 9$, and $P < 0.001$) reflects the dominant high biogenic carbonate content. The high negative loading of PC1 in $SiOB_{2B}$, $AlB_{2B}OB_{3B}$, $FeB_{2B}OB_{3B}$, MgO and $TiOB_{2B}$ reflects the presence of serpentine, talc and possibly rock-fragments-derived components. Sample SCD7 clearly plots at more negative values than the remaining samples, in accordance with the absence of a biogenic component and the presence of serpentine and talc. Calcium concentrations in SCD7 are much lower (average = 5.14 ± 2.32%) than in the other cores (average = 33.82 ± 2.19%) and the strong positive correlation between Ca and C downcore ($r = 0.99$, $N = 11$, $P < 0.001$; Fig. 4A) and the absence of foraminiferal tests indicate that the main source of Ca and C in this sediment is hydrothermal calcite. Silica (15.5%–22.1%) and Mg (12.2%–17.7%) are the major elements in the SCD7 sediment. Talc and serpentine (and minor chlorite) are the main phyllosilicates and are the principal source of Mg in the bulk sediment. Unlike the other samples, downcore Si variations in SCD7 are negatively correlated with Al (SCD7: $r = -0.71$, $N = 11$, $P = 0.001$; remaining samples: $r = 0.91$, $N = 9$, and $P = 0.001$), and the Si/Al ratios are particularly high (9.2–27 in the 13–27 cmbsf layer; Fig. 4B), suggesting a hydrothermal input of silica. The relatively immobile elements Ti and Al are present in lithogenic components and are correlated downcore in SCD7 ($r = 0.99$, $N = 11$ and $P < 0.001$; Fig. 4C). The highest contents occur at the top (0–8 cmbsf: Al = 6.01–6.86% and Ti = 0.50–0.56%), consistent with the presence of lithoclasts in these layers. Ti and Al concentrations decrease significantly downcore, with the lowest contents in layers where hydrothermal components are more abundant (16–21 cmbsf: Al = 0.66%–1.37% and Ti = 0.02%–0.06%). Below these layers the Ti and Al contents increase again, although with a lower concentration than at the top (Al = 0.65%–2.34% and Ti = 0.02%–0.08%) and correspond to an increase in rock-fragments constituents.

In the PCA for major oxides, vector PC2 accounts for 19.7% of the variance and has a high positive loading for MnO (Fig. 3A). Samples SH63T, SH118T and SH119, collected directly at the vent orifices (inside the circle in Fig. 3), project at high PC2 values as a consequence of higher MnO contents (see Electronic Supplementary Data). The higher average Mn/Fe ratios in these samples (9.86, 3.41 and 2.42, respectively) reflect higher concentrations of hydrothermal oxyhydroxides, which typically precipitate at lower temperatures. Of these three cores, analyses of profiles with depth were only possible for SH119. This core has the highest Mn concentrations at the top (0–6 cmbsf), with Mn/Fe ratios ranging from 3.0 to 8.1 and decreasing to 0.17 to 0.36 in the bottom layers. This suggests that oxyhydroxides precipitate directly at the subsurface due to cooling and gradually more oxidizing conditions that result from mixing with seawater (Krauskopf, 1957). Because Fe^{2+} precipitation is favored at lower Eh and pH conditions than Mn^{2+}, the chemical gradient established during fluid ascent favors Fe precipitation at deeper layers and Mn precipitation closer to the surface leading to the changing Fe/Mn ratios (Boström and Peterson, 1969; Corliss et al., 1978).

In the PCA for trace elements SCD7 also projects apart from the other samples (Fig. 3B). PC1 accounts for 73% of the variance and has high loadings for Fe, Zn, Cu, Ni, Co, Cr, V, and Sc. The SCD7 sediment is enriched in these elements compared to the other cores and they are essentially incorporated in hydrothermal sulphides, as well as in serpentine and talc. In SCD7 S, Cu, Fe and Zn concentrations fluctuate downcore due to the variable proportions of rock fragments and hydrothermal overprint. In general, their concentration is higher below 9–10 cmbsf and particularly enriched between 13 and 21 cmbsf. Other elements such as Ni, Co and Cr in core SCD7 follow

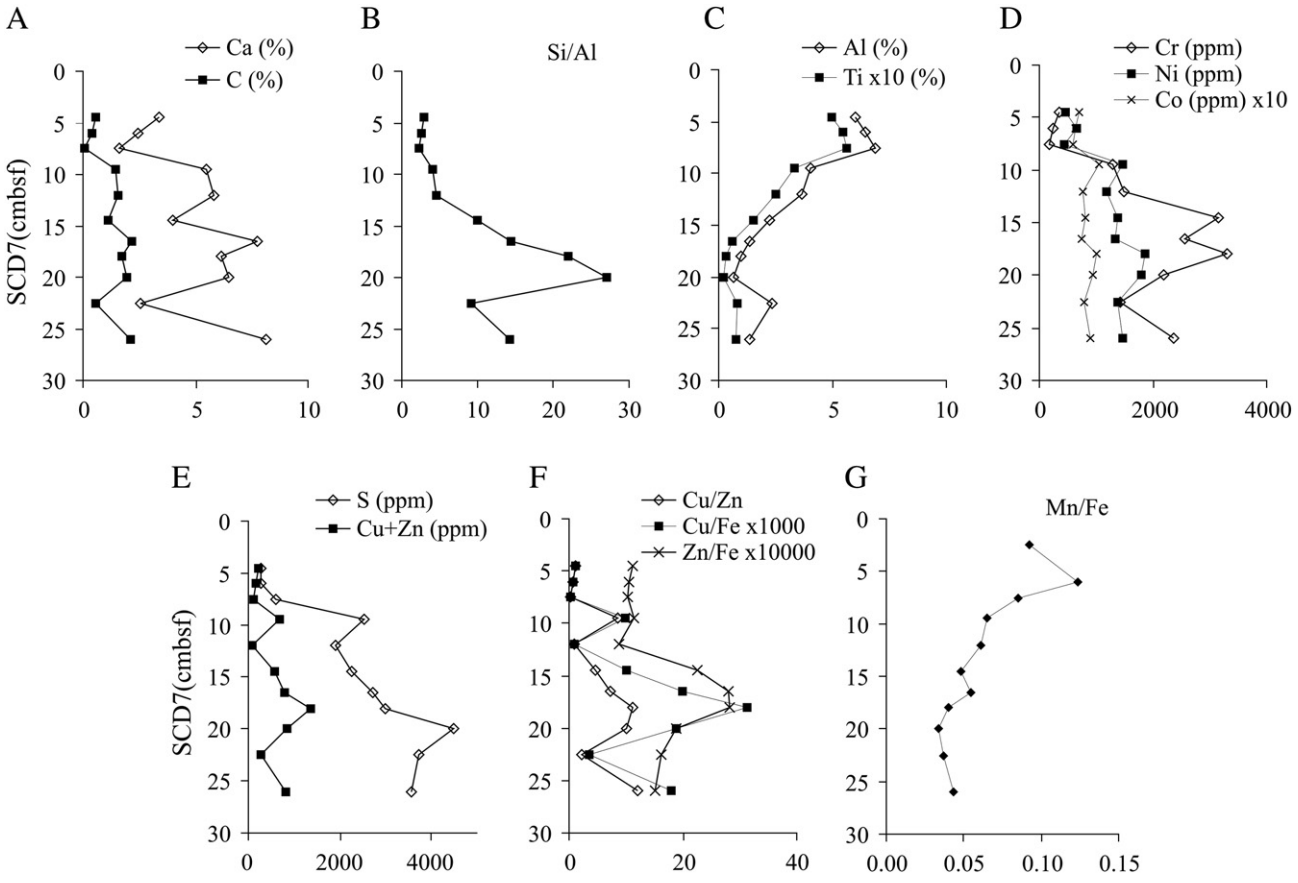

Fig. 4. SCD7 sediment core downcore variation in (A) Ca and C; (B) Si/Al; (C) Al and Ti; (D) Cr, Ni and Co × 10; (E) S and Cu + Zn; (F) Cu/Zn, Cu/Fe*1000 and Zn/Fe*10000; and (G) Mn/Fe.

a similar pattern (Fig. 4D). The presence of these elements in SCD7 may either reflect the occurrence of ultramafic-derived fragments in the sediment and/or the influence of hydrothermal fluids. The S and Cu + Zn concentrations correlate downcore ($r = 0.64$, $N = 11$, and $P = 0.035$) as these elements are incorporated in sulphides (Fig. 4E). However, effective separation of Cu, Zn, Fe and Mn occurs downcore, as revealed by the increasing ratios of Cu/Zn, Cu/Fe and Zn/Fe (Fig. 4F) and decreasing ratios of Mn/Fe (Fig. 4G). The precipitation of Cu, followed by Zn and Fe and finally by Mn, from the lower to the upper sediment layers, may be caused by cooling and by the chemical gradient along the ascent path of the high-temperature hydrothermal fluid. Under these conditions, the precipitation of Cu-sulphides occurs at depth followed by Cu–Zn and Fe sulphides. In contrast to the other sediment cores that are mainly enriched in Mn, only a slight Mn enrichment is observed at the very top of the SCD7 core. We suggest that this is a consequence of the higher fluid oxidation, where Mn and the remaining Fe (not incorporated into sulphide phases) precipitate to form the rare Mn-oxyhydroxides. V is typically derived from seawater and is slightly enriched in the upper layers of SCD7, suggesting more extensive seawater mixing in the superficial layers and co-precipitation with oxyhydroxides (Feely et al., 1989; German et al., 2002).

PC2 for trace elements accounts for 12.5% of the variance and has high negative loadings for S and U, reflecting their high concentrations in sediments directly collected at vent orifices (SH63T, SH119 and SH118T). Uranium is probably scavenged from seawater by hydrothermal sulphide (German et al., 2002). Sample S118T projects closer to sediments collected away from the vent area. This is the consequence of the Fe–Mn crust that reduced the interaction with seawater. Sediments far from the vent area plot at positive values of PC2 reflecting the higher contents in V and Th. In both the major oxides and trace elements analyses, sample SH49, collected at the vent area but away from the vent orifices (Fig. 3A and 3B), shows a negligible hydrothermal contribution. This suggests that hydrothermal precipitation is only significant when hydrothermal fluid flow is focused.

4.2.2. REE contents

Variation in rare earth elements (REE) concentrations are listed in the Electronic Supplementary Data, along with the $(La/Sm)B_{CNB}$, $(Gd/Yb)B_{CN}$, and $(La/Yb)B_{CNB}$ ratios, and the Ce and Eu anomalies. REE normalized patterns for chondrites (CN: Taylor and McLennan, 1985) are presented in Fig. 5. With the exception of SCD7, all cores show similar REE patterns with depth and, thus, we only present average values for each core (Fig. 5A). Samples collected directly at the vent orifices have REE patterns essentially indistinct from the remaining cores, with a depletion in HREE (heavy rare earth elements) and a negative Ce ($(Ce/Ce^*)B_{CNB}$ average = 0.60) and a slightly negative Eu anomaly ($(Eu/Eu^*)B_{CNB}$ average = 0.77). This pattern is comparable with that of pelagic sediments, although with more pronounced Ce negative anomalies as consequence of REE scavenging from seawater, probably by Fe–Mn oxyhydroxides precipitated by low-temperature fluids. These results are compatible to those of Dias and Barriga, 2006).

Core SCD7 exhibits distinctive REE patterns. In general, the sediment shows: (1) a decrease of REE values from the top to the base of the core; (2) a flat REE pattern with a pronounced negative Eu anomaly and ten times higher REE contents than chondrite above 8 cmbsf; (3) a positive Eu anomaly with a LREE enrichment between 16–21 cmbsf, reflecting a hydrothermal contribution; (4) a pattern similar to the top layers below 22 cmbsf, although with lower REE concentrations; and (5) between 8–16 cmbsf, an evident mixing of REE from layers above and below (Fig. 5B).

The depth-variation in REE is essentially related to the varying proportions of rock fragments and hydrothermal components. The downcore REE decrease could thus reflect increasing hydrothermal overprint in the deeper layers because hydrothermal fluids have lower REE concentrations. However, the depletion of REE content in the SCD7 core could also be related to the abundance of talc, serpentine and chlorite that characteristically incorporate minimal quantities of REE in their crystal lattice (Gillis et al., 1992). In the deeper layers, especially between 13 and 21 cmbsf, the distinct hydrothermal REE signature reflects the higher amounts of sulphides and hydrothermal calcite in a talc and serpentine background and a lower amount of rock fragments. The positive Eu anomaly ($(Eu/Eu^*)B_{CNB} = 1.30–1.68$) with a LREE enrichment between 16 and 21 cmbsf are consistent with mineral precipitation from a high-temperature fluid (>250 °C) under highly reducing conditions and high ClP^{-P} contents (Allen and Seyfried, 2005; Klinkhammer et al., 1994; Michard, 1989; Sverjensky, 1984). Europium anomalies of comparable magnitude were described for hydrothermal sediments from high-temperature hydrothermal fields such as TAG (Fig. 6), where the

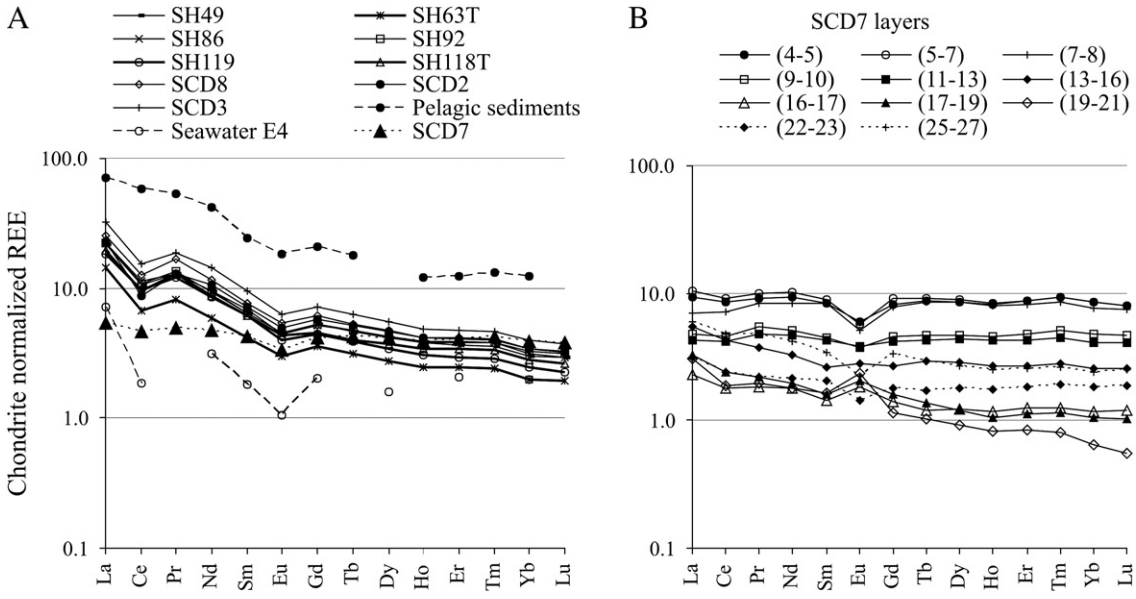

Fig. 5. Average chondrite-normalized (Taylor and McLennan, 1985) REE values for: (A) Saldanha core sediments, deep (1500–2500 m) seawater (Elderfield and Greaves, 1982) and pelagic sediments (Wildeman and Haskin, 1965); (B) SCD7 sediment layers.

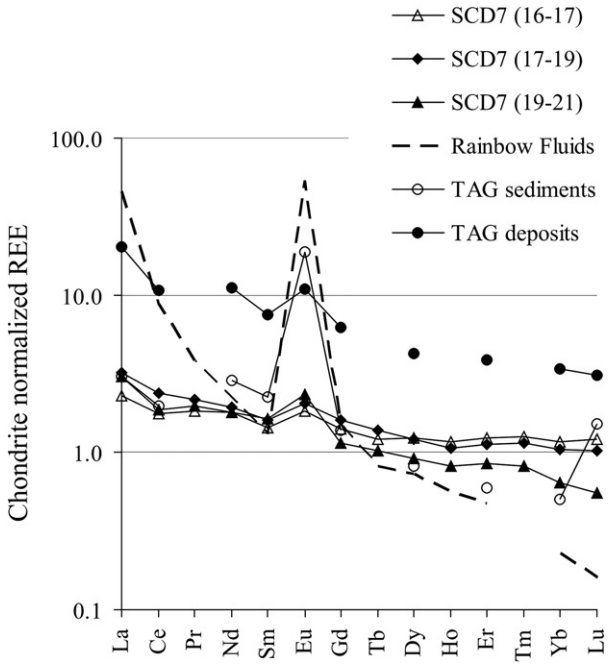

Fig. 6. Chondrite-normalized (Taylor and McLennan, 1985) REE patterns from the SCD7 sediment layers with stronger hydrothermal signatures. Patterns from Rainbow hydrothermal fluids (Douville et al., 2002), as well as average values from TAG metalliferous sediments (German et al., 1993) and from TAG hydrothermal deposits (Mills and Elderfield, 1995b) are also presented for comparison.

$(Eu/Eu^*)B_{CNB}$ average varies between 1.57 and 1.76 (German et al., 1993; Mills et al., 1993).

The flat pattern with a negative Eu anomaly recorded in layers above 8 cmbsf and below 22 cmbsf correlates with the presence of talc. Studies of talc from abyssal peridotites recovered on ODP Leg 209 (Mid-Atlantic Ridge 15°20′ N) indicated pronounced negative Eu anomalies and flat to LREE enriched patterns (Paulick et al., 2006).

A comparison of the SCD7 REE pattern with those described for hydrothermal fluids (Fig. 6) further supports our interpretation that the enrichment in LREE and the pronounced positive Eu anomaly in this core are derived from hydrothermal fluids. REE derived from unaltered seawater in this core are low, as suggested by the low negative Ce anomaly.

4.3. Stable isotope geochemistry

Oxygen and carbon isotope analyses of carbonates of the three cores collected directly at the vent orifices, for core SCD7 and for two cores collected away from the vent area are presented in Table 3 and in Fig. 7. The majority of Saldanha bulk carbonates have $\delta P^{18P}O$ (VSMOW) $_B$values ranging from 30.2‰ to 34.2‰ and reflect a dominant pelagic carbonate source.

Sample SCD7 shows much lower $\delta P^{18P}O$ values ranging from 12.7‰ to 16.0‰ pointing to high-temperature alteration at temperatures in the range of 112–150 °C. Isotopic analyses of isolated hydrothermal calcite crystals in sample SCD7 yielded $\delta P^{18P}O_{(VSMOW)}$ values of 6.6–11.6‰, indicating temperatures of up to 260 °C. For these temperatures estimates, the calcite–water fractionation factor of Friedman and O´Neil (1977) was used, assuming an unmodified

Table 3
Stable isotope compositions of Saldanha bulk sediment samples and of hydrothermal calcite isolated from sample SCD7. Temperature estimates for each sample are also presented.

	cmbsf	$\delta^{18}O_{(VPDB)}$	$\delta^{18}O_{(VSMOW)}$	$\delta^{18}C_{(VPDB)}$	Min. T (°C)*(1)	T (°C)*(2)	Max. T (°C)*(3)
Bulk sediment							
SH63T		1.0	31.9	0.4	12	16	20
SH92	2–3	1.1	32.0	−0.2	11	15	20
	6–7	1.2	32.2	0.0	10	15	19
	10–11	1.7	32.6	0.3	9	13	17
SH118T		0.7	31.6	0.2	13	17	22
SH119	2–3	0.9	31.9	−0.1	12	16	21
	4–5	1.6	32.6	−0.2	9	13	17
	6–7	2.2	33.2	−0.2	7	11	15
	8–9	1.5	32.4	−0.2	10	14	18
SCD7	7–8	−14.5	16.0	−2.0	112	123	134
	9–10	−16.6	13.8	−4.2	136	149	164
	11–13	−17.6	12.7	−2.5	150	164	180
	16–17	−15.6	14.8	−2.4	125	136	149
	19–21	−15.8	14.6	−3.3	126	138	151
	22–23	−15.0	15.5	−4.0	117	128	141
	25–27	−17.2	13.2	−1.4	144	158	173
SCD8	0–2	2.0	33.0	0.0	7	11	16
	4–6	1.9	32.8	0.1	8	12	16
	8–10	−0.1	30.8	−4.5	16	21	25
	12–14	−0.6	30.2	−6.4	19	23	28
	20–22	1.9	32.9	0.3	8	12	16
	40–42	3.2	34.2	0.5	3	7	11
	88–90	2.1	33.1	0.1	7	11	15
Calcite							
SCD7	6–8	−23.6	6.6	−3.3	269	300	337
	9–10	−21.6	8.6	−2.7	219	241	268
	11–13	−21.0	9.3	−1.8	206	227	251
	13–16	−21.3	9.0	−3.1	212	234	259
	16–17	−21.9	8.3	−1.7	226	249	277
	17–19	−18.7	11.6	−0.9	165	181	199
	19–21	−20.8	9.5	−0.6	202	223	246
	22–23	−20.1	10.2	−1.3	188	207	228
	23–25	−21.0	9.3	−0.8	205	227	251
	25–27	−21.8	8.5	−1.5	222	246	273

(*) Temperature estimation was based on the calcite-water fractionation factor of Friedman and O'Neil (1977), assuming seawater $\delta P18PO\ B(SMOW)B$ values of (1) 0‰; (2) 1‰ and; (3) 2‰.

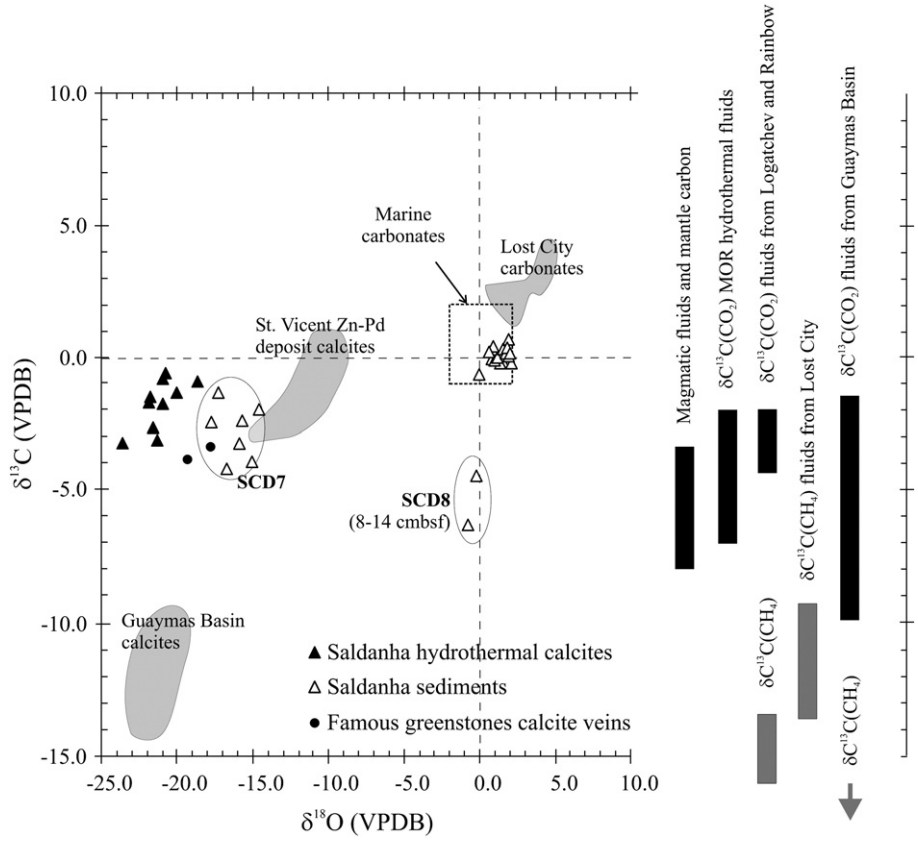

Fig. 7. Plot of $\delta P^{13P}C$ vs. $\delta P^{16P}O$ values of Saldanha sediments and hydrothermal calcites. For comparison, values of hydrothermal calcites associated with ore forming hydrothermal systems (Zn–Pb deposits from St Vicent, Peru: Spangenberg et al., 1996; Guayamas Basin: Peter and Shanks, 1992), FAMOUS greenstones calcite veins (Stakes and Oneil, 1982) and carbonates from Lost City (Früh-Green et al., 2003) are also projected. The right-hand side of the diagram shows the ranges of PC and O isotopic values for marine limestones (Ohmoto, 1986; Ohmoto and Goldhaber, 1997), magmatic fluids and mantle degassing (Anderson and Arthur, 1983; Gerlach and Taylor, 1990; Hoefs, 1997; Taylor, 1986; Zheng and Hoefs, 1993), and hydrothermal fluids from Rainbow and Logatchev (Charlou et al., 2000), Lost City (Proskurowski et al., 2008) and from the Guayamas Basin sedimented ridge system, with a high organic matter content (Welhan and Lupton, 1987).

seawater $\delta P^{18P}O$ $B_{(SMOW)B} = 0‰$. However, because oxygen isotopic determination in hydrothermal fluids show values ranging between 0 and 2‰ (e.g., Shanks et al., 1995 and references therein), calculations were also performed assuming modified seawater $\delta P^{18P}O$ $B_{(SMOW)}$ values of 1‰ and 2‰ (Table 3). These calculations yielded values of 300 °C (1‰) and 337 °C (2‰) for SCD7 calcite precipitation temperatures. These temperatures are consistent with the high temperatures (>250 °C) suggested by the presence of sulphides. The lower temperatures obtained for the bulk sediment of SCD7 is due to the presence of pelagic carbonate, formed at lower temperatures.

All samples, with the exception of SCD7 and layers between 8–14 cmbsf of SCD8, show $\delta P^{13P}C$ values from −0.2 to 0.5‰, in the range of normal marine carbonates (−1 to 2‰; Ohmoto, 1986; Ohmoto and Goldhaber, 1997). The SCD7 samples show a clear depletion in $P^{13P}C$, with values ranging from −4.3 to −1.4‰ in bulk sediment and from −3.3 to −0.6‰ in isolated calcites (Table 3). A plot of $\delta P^{13P}C$ vs. $s\delta P^{18P}O$ (Fig. 7) shows that Saldanha sediments, except for SCD7, plot in the field for normal marine carbonates with values similar to pelagic limestones from Lost City (Früh-Green et al., 2003). SCD7, on the other hand, plots close to values from calcite veins from FAMOUS greenstone breccias (Stakes and Oneil, 1982) and to hydrothermal calcites of the San Vicente deposit (Spangenberg et al., 1996). Although the San Vicente deposit is located on land, it contains hydrothermal calcites associated with Zn-sulphide mineralization, as in Saldanha (Fig. 7). The C-isotope compositions of the SCD7 samples lie within the range considered for mantle carbon ($\delta P^{13P}C$: −8 to −3.4‰, e.g., Gerlach and Taylor, 1990; Hoefs, 1997; Ohmoto and Goldhaber, 1997; Taylor, 1986; Zheng and Hoefs, 1993). Thus, the association of Zn-sulphides and calcite and the ^{12}C-depleted compositions of the calcite are consistent with a magmatic CO_2 component in the hydrothermal fluids. The calcites in SCD7 may have precipitated as a consequence of CO_2 degassing and concomitant pH increase of a slightly acidic ore fluid (Spangenberg et al., 1996). Carbon derived from the oxidation of sedimentary organic carbon and/or hydrothermal methane is also a possible alternative. With the available data it is not possible to unequivocally distinguish between these possible sources. However, the lack of strongly negative values as observed for example in the organic-rich sediments in the Guaymas basin, suggests that the mantle C may be a more likely source.

In high-temperature hydrothermal systems, degassing of magmatic COB_{2B} is a major source of carbon in hydrothermal fluids (e.g., Proskurowski et al., 2004) and could be an effective process leading to the precipitation of calcite (Zheng, 1990). The SCD7 downcore variation in the isotopic composition of calcites may reflect the interaction of carbonate ooze with the hydrothermal fluid or different degrees of mixing of fluids with different isotopic compositions (hydrothermal fluids and fresh seawater).

Hydrothermal fluids from Logatchev and Rainbow have similar $\delta P^{13P}C$ signatures of CO_2 as those recorded at SCD7 (see Fig. 7) and are considered systems with seawater circulation through ultramafic basement rocks but with a magmatic contribution (Charlou et al., 2002; Douville et al., 2002). Because Saldanha has similar basement lithologies and lies in a similar geologic framework, we can envision a similar origin of the hydrothermal fluids as those at Logatchev and Rainbow. At Lost City, on the other hand, abiotic methane is the dominant carbon species in the fluids and is believed to form abiotically through reduction of mantle carbon by Fischer Tropsch-type reactions during serpentinization (Proskurowski et al., 2008).

There is no or negligible CO_2 in the Lost City fluids, which reflects the high pH that is characteristic of this system. The Lost City hydrothermal carbonate deposits and their carbon isotope signatures reflect primarily a marine source of carbon and deposition as a result of mixing of high pH, hydrothermal fluids with seawater (Früh-Green et al., 2003; Kelley et al., 2005; Proskurowski et al., 2008). Thus, on the basis of stable isotopes alone, the source of carbon in the hydrothermally altered Saldanha sediments remains equivocal.

Core SCD8, collected far from the summit, reveals a wide range of $\delta P^{13P}C$ values for the bulk sediment, ranging from typical marine sediment values to values as low as −6.5‰ in layers between 8–14 cmbsf (Table 3). Although in this sediment there is no other clear geochemical evidence for hydrothermal activity, the $\delta P^{13P}C$ values in these layers could indicate minor hydrothermal overprinting. This is consistent with oxygen-isotope derived temperatures, which are highest (16 to18°C) in those layers. If these signatures are related to hydrothermal activity, this suggests a contribution by lateral flow of hydrothermal fluids at depth or earlier episodes of hydrothermal activity far from the Saldanha vent area. Further analyses from samples collected in that area are necessary to better constrain the origin of the hydrothermal component.

5. Conclusions

The Saldanha sediments are dominated by biogenic carbonate with variable rock fragment components and with a minor hydrothermal input. In general, hydrothermal phases are derived from low-temperature hydrothermal fluids and are characterized by Mn and Fe oxyhydroxides and minor amounts of sulphide precipitates. The exception to this pattern is the SCD7 sediment core that records strong hydrothermal overprinting and a negligible biogenic fraction.

Geochemical and isotopic analyses on the SCD7 core suggest mineral precipitation from high-temperature (>250 °C) fluids. The SCD7 downcore variation in Cu/Zn, Cu/Fe, Zn/Fe and Mn/Fe ratios is consistent with an effective separation of these metals during gradual cooling, and concomitant Eh and pH modifications, as discharging high-temperature fluids interact with the background sediment and mix with seawater. This promotes the precipitation of Cu-sulphides at depth, followed by Cu–Zn and Fe sulphides and of Fe–Mn oxyhydroxides at the top. The sulphide assemblage recorded in this core (chalcopyrite + sphalerite/wurtzite ± pyrite–pyrrhotite) and the observed positive Eu anomaly associated with LREE enrichments is consistent with precipitation from high-temperature fluids and with interaction of the hydrothermal fluid with mafic rocks. In accordance, O and C isotopic data from SCD7 carbonates indicate that high-temperature fluids (260 °C–330 °C) have been involved in their precipitation, controlled by changes of Eh, pH and temperature of the fluid during interaction with the hosted carbonated oozes with variable mixing with seawater. The low values of $\delta P^{13P}C$ of this core also point to a magmatic and/or biogenic carbon component in hydrothermal fluids in Saldanha system. Degassing processes may be the principal source of COB_2 to the Saldanha fluids although CH_4 produced through serpentinization reactions may also be present, as is observed in the Logatchev and Rainbow fluids.

Taken together, the data suggest that at Saldanha mineralization occurs in the shallow subsurface by the interaction of hydrothermal fluids with the sediment cover and seawater. Higher amount of sulphides and hydrothermal calcite precipitation in the SCD7 sediment core suggest the presence of more focused and higher temperature fluids, which are likely related to the fault network in the Saldanha area. Therefore, channelled fluids are vented at the seafloor with much higher temperatures than those directly measured at the vent orifices where samples SH63T, SH118T and SH119 were collected. The exposure of serpentinites and steatites within the Saldanha massif also appears to be linked with the faulting network. We propose that seawater descends through the crust reacting with mafic rocks and ascends along the faults at the top of the massif, reacting with ultramafic rocks. Thus, a convective hydrothermal circulation system in the Saldanha field, with hydrothermal precipitation in the subsurface and discharge zone at the top of the Saldanha mount seems likely.

The high-temperature mineral assemblage of SCD7 sediment core suggests that the heat source for the Saldanha hydrothermal system is most probably magmatic, although heat derived by lithospheric cooling and by serpentinization exothermic reactions may also contribute to the system.

Acknowledgements

We thank all participants in the Saldanha 1998, Seahma 2001 and CD167 cruises for various forms of indispensable cooperation in surveying and sampling. Miguel Bassa Pacheco for helping with ArcGis software digital elevation models (DEMs). We also acknowledge financial support from FCT (Portugal) through Ágata Dias (SFRH/BD/8896/2002) and through AMAR-Praxis XXI (2/2.1/MAR/1743/95) and SEAHMA (POCTI/MAR/15281/1999-FEDER) projects and from UK Natural Environment Research Council and through a PhD scholarship. We also thank the editor of Marine Geology, David J.W. Piper, and two anonymous reviewers for their helpful comments and suggestions.

Appendix A. Supplementary data

Supplementary data to this article can be found online at doi:10.1016/j.margeo.2010.10.017.

References

Allen, D.E., Seyfried Jr., W.E., 2003. Compositional controls on vent fluids from ultramafic-hosted hydrothermal systems at mid-ocean ridges: An experimental study at 400 °C, 500 bars. Geochimica et Cosmochimica Acta 67 (8), 1531–1542.
Allen, D.E., Seyfried Jr., W.E., 2004. Serpentinization and heat generation: Constraints from Lost City and Rainbow hydrothermal systems. Geochimica et Cosmochimica Acta 68 (6), 1347–1354.
Allen, D.E., Seyfried Jr., W.E., 2005. REE controls in ultramafic hosted MOR hydrothermal systems: An experimental study at elevated temperature and pressure. Geochimica et Cosmochimica Acta 69 (3), 675–683.
Alt, J.C., Teagle, D.A.H., Brewer, T., Shanks III, E.C., Halliday, A., 1998. Sulfur in serpentinized oceanic peridotites: Serpentinization processes and microbial sulfate reduction. Journal of Geophysical Research 103 (B5), 9917–9929.
Anderson, T.F., Arthur, M.A., 1983. Stable isotopes of oxygen and carbon and their applications to sedimentologic and paleoenvironmental problems. In: Arthur, M.A., Anderson, T.F., Kaplan, I.F., Veizer, J., Land, L.S. (Eds.), Stable Isotopes in Sedimentary Geology. SEPM Short Course.
Bach, W., Banerjee, N.R., Dick, H.J.B., Baker, E.T., 2002. Discovery of ancient and active hydrothermal systems along the ultra-slow spreading Southwest Indian Ridge 10°–16°E. Geochemistry Geophysics Geosystems 3 (7), 21p.
Bach, W., Garrido, C.J., Paulick, H., Harvey, J., Rosner, M., 2004. Seawater-peridotite interactions: First insights from ODP Leg 209, MAR 15° N. Geochemistry Geophysics Geosystems 5 (9), Q09F26.
Barriga, F.J.A.S., Fouquet, Y., Almeida, A., Biscoito, M., Charlou, J.-L., Costa, R.P.C., et al., 1998. Discovery of the Saldanha hydrothermal field on the FAMOUS segment of the MAR (36º 30'N). Eos, Transactions, American Geophysical Union 79 (45), F67.
Barriga, F.J.A.S., Almeida, A., Biscoito, M., Colaço, A., Company, R., Costa, R., et al., 2003. Seahma-1 Cruise Report Faculty of Sciences. University of Lisbon, Lisbon.
Barriga, F.J.A.S., Dias, A., Marques, A., Relvas, J., Miranda, J.M., Queiroz, G., et al., 2004. Mount Saldanha revisited: low-temperature methane discharge through a sediment-capped serpentinite protrusion (MoMAR Area, Mid-Atlantic Ridge, 36°30′N), European Geosciences Union 1st General Assembly, Nice.
Ben Othman, D., White, W.M., Patchett, J., 1989. The geochemistry of marine sediments, island arc magma genesis, and crust-mantle recycling. Earth and Planetary Science Letters 94 (1–2), 1–21.
Bogdanov, Y.A., Bortnikov, N.S., Vikentev, I.V., Gurvich, E.G., Sagalevich, A.M., 1997. New type of the modern mineral-forming system: black smokers of the hydrothermal field 14o45' N, MAR. Geology of Ore Deposits 39 (1), 58–78.
Bonatti, E., 1981. Metal deposits in the oceanic lithosphere. In: Emiliani, C. (Ed.), The Sea. Wiley & Sons, New York, pp. 639–686.
Bonatti, E., Joensuu, O., 1966. Deep sea iron deposits from the South Pacific. Science 154, 643–645.
Boschi, C., Fruh-Green, G.L., Delacour, A., Karson, J.A., Kelley, D.S., 2006a. Mass transfer and fluid flow during detachment faulting and development of an oceanic core

complex, Atlantis Massif (MAR 30 degrees N). Geochemistry Geophysics Geosystems 7.
Boschi, C., Fruh-Green, G.L., Escartin, J., 2006b. Occurrence and significance of serpentinite-hosted, talc- and amphibole-rich fault rocks in modern oceanic settings and ophiolite complexes: An overview. Ofioliti 31 (2), 129–140.
Boström, K., Peterson, N.N.A., 1966. Precipitates from hydrothermal exhalations on the East Pacific Rise. Economic Geology 61, 1258–1265.
Boström, K., Peterson, S., 1969. The origin of aluminium-poor ferromanganoan sediments in areas of areas of high heat flow on the East Pacific Rise. Marine Geology 7 (5), 427–447.
Bougault, H., Aballéa, M., Radford-Knoery, J., Charlou, J.-L., Baptiste, P.J., Appriou, P., et al., 1998. FAMOUS and AMAR segment on the Mid-Atlantic Ridge: Ubiquitous hydrothermal Mn, CH_4, δ^3He signals along the rift valley walls and rift offsets. Earth and Planetary Science Letters 161, 1–17.
Brazelton, W.J., Schrenk, M.O., Kelley, D.S., Baross, J.A., 2006. Methane- and sulfur-metabolizing microbial communities dominate the Lost City hydrothermal field ecosystem. Applied and Environmental Microbiology 72 (9), 6257–6270.
Calvert, S.E., Price, N.B., 1970. Composition of manganese nodules and manganese carbonates from Loch Fyne, Scotland. Contributions to Mineralogy and Petrology 29, 215–233.
Cannat, M., 1993. Emplacement of mantle rocks in the sea-floor at Mid-Ocean Ridges. Journal of Geophysical Research-Solid Earth 98 (B3), 4163–4172.
Cannat, M., Mevel, C., Maia, M., Deplus, C., Durand, C., Gente, P., et al., 1995. Thin crust, ultramafic exposures, and rugged faulting patterns at Mid-Atlantic Ridge (22º - 24ºN). Geology 23 (1), 49–52.
Cave, R.R., German, C.R., Thomson, J., Nesbitt, R.W., 2002. Fluxes to sediments underlying the Rainbow hydrothermal plume at 36°14'N on the Mid-Atlantic Ridge. Geochimica et Cosmochimica Acta 66 (11), 1905–1923.
Charlou, J.L., Bougault, H., Donval, J., Pelle´, P.H., Langmuir, C., Team, F.S., 1993. Seawater CH_4 concentration over the Mid-Atlantic Ridge from the Hayes F.Z. to the Azores triple junction. Eos 74, 380.
Charlou, J.-L., Donval, J.-P., Douville, E., Knoery, J., Fouquet, Y., Bougault, H., et al., 1997. High methane flux between 15ºN and the Azores Triple Junction, Mid-Atlantic ridge, hydrothermal and serpentinization processes. Eos, Transactions, American Geophysical Union 78 (F831).
Charlou, J.L., Donval, J.P., Douville, E., Jean-Baptiste, P., Radford-Knoery, J., Fouquet, Y., et al., 2000. Compared geochemical signatures and the evolution of Menez Gwen (37°50'N) and Lucky Strike (37°17'N) hydrothermal fluids, south of the Azores Triple Junction on the Mid-Atlantic Ridge. Chemical Geology 171 (1–2), 49–75.
Charlou, J.-L., Donval, J.-P., Fouquet, Y., Jean-Baptiste, P., Holm, N.G., 2002. Geochemistry of high H_2 and CH_4 vent fluids issuing from ultramafic rocks at the Rainbow hydrothermal field (36º14'N, MAR). Chemical Geology 191, 345–359.
Chavagnac, V., Palmer, M.R., Milton, J.A., Green, D.R.H., German, C.R., 2006. Hydrothermal sediments as a potential record of seawater Nd isotope compositions: The Rainbow vent site (36°14' N, Mid-Atlantic Ridge). Paleoceanography 21 (3), PA3012.
Coplen, T.B., Kendall, C., Hopple, J., 1983. Comparison of stable isotope reference samples. Nature 302 (5905), 236–238.
Corliss, J.B., Lyle, M., Dymond, J., Crane, K., 1978. The chemistry of hydrothermal mounds near the Galapagos rift. Earth and Planetary Science Letters 40, 12–24.
Dias, Á.S., Barriga, F.J.A.S., 2005. Mineralogical and geochemical hydrothermal evidences on sediments from the serpentinite-hosted Saldanha hydrothermal field. In: Mao, J., Bierlein, F.P. (Eds.), Mineral Deposit Research: Meeting the Global Challenge, Vols 1 and 2, pp. 603–606.
Dias, A., Barriga, F., 2006. Mineralogy and geochemistry of hydrothermal sediments from the serpentinite-hosted Saldanha hydrothermal field (36º34'N; 33º26'W) at MAR. Marine Geology 225, 157–175.
Dias, A., Jorge, R.C.G.S., Barriga, F.J.A.S., 2005. Low temperature hydrothermal Manganese crust from Saldanha field, Mid-Atlantic Ridge, International MoMAR Implementation Workshop, 7–9 April 2005, Lisbon, Portugal, p. 29.
Dias, Á.S., Mills, R.A., Ribeiro da Costa, I., Costa, R., Taylor, R.N., Cooper, M.J., et al., 2010. Tracing fluid–rock reaction and hydrothermal circulation at the Saldanha hydrothermal field. Chemical Geology 273 (3–4), 168–179.
Dick, H.J.B., Tivey, M.A., Tucholke, B.E., 2008. Plutonic foundation of a slow-spreading ridge segment: Oceanic core complex at Kane Megamullion, 23°30'N, 45°20'W. Geochemistry Geophysics Geosystems 9.
Douville, E., Charlou, J.L., Oelkers, E.H., Bienvenu, P., Jove Colon, C.F., Donval, J.P., et al., 2002. The Rainbow vent fluids (36º14'N, MAR): The influence of ultramafic rocks and phase separation on trace metal content in Mid-Atlantic Ridge hydrothermal fluids. Chemical Geology 184 (1–2), 37–48.
Dyment, J., ArkaniHamed, J., Ghods, A., 1997. Contribution of serpentinized ultramafics to marine magnetic anomalies at slow and intermediate spreading centres: Insights from the shape of the anomalies. Geophysical Journal International 129 (3), 691–701.
Dzhatieva, Z., Sinha, M., Santos, F., Dean, S., Dias, A., Marques, A., et al., 2005. Active source electromagnetic survey of hydrothermal venting area at Saldanha Massif, Mid-Atlantic Ridge—The CD 167/2004 cruise. InterRidge News.
Edmonds, H., German, C., 2004. Particle geochemistry in the Rainbow hydrothermal plume, Mid-Atlantic Ridge. Geochimica et Cosmochimica Acta 68 (4), 759–772.
Elderfield, H., Greaves, M.J., 1982. The rare earth elements in seawater. Nature 18, 214–219.
Escartin, J., Cannat, M., 1999. Ultramafic exposures and the gravity signature of the lithosphere near the Fifteen-Twenty Fracture Zone (Mid-Atlantic Ridge, 14°–16.5° N). Earth and Planetary Science Letters 171 (3), 411–424.
Escartin, J., Mevel, C., MacLeod, C.J., McCaig, A.M., 2003. Constraints on deformation conditions and the origin of oceanic detachments: The Mid-Atlantic Ridge core complex at 15 degrees 45'N. Geochemistry Geophysics Geosystems 4.
Escartín, J., Hirth, G., Evans, B., 1997. Effects of serpentinization on the lithospheric strength and the style of normal faulting at slow-spreading ridges. Earth and Planetary Science Letters 151, 181–189.
Faure, G., 1986. Principles of isotope geology. John Wiley & Sons. 589 pp.
Feely, R.A., Massoth, G.J., Trefry, J.H., 1989. The role of Fe oxyhydroxides in Phosphorus, Vanadium and Arsenic Scavenging over the Mid-Atlantic Ridge and Juan-de-Fuca Ridge hydrothermal systems. Abstracts of Papers of the American Chemical Society 198, 102-GEOC.
Fouquet, Y., Charlou, J.-L., Ondréas, H., Radford-Knoery, J., Donval, J.-P., Douville, E., et al., 1997. Discovery and first submergible investigations on the Rainbow hydrothermal field on the MAR (36º 14N). Eos, Transactions, American Geophysical Union 78 (F832).
Fouquet, Y., Barriga, F.J.A.S., Charlou, J.-L., Elderfield, H., German, C.R., Ondréas, H., et al., 1998. FLORES diving cruise with the Nautile near Azores - First dives on Rainbow field: Hydrothermal seawater/mantle interaction. Inter Ridge News 7 (1), 1998.
Friedman, I., O´Neil, J., 1977. Compilation of stable isotope fractionation factors of geochemical interest. In: Fleischer, M. (Ed.), Data in Geochemistry. Geological Survey Professional Paper, p. 12.
Früh-Green, G.L., Kelley, D.S., Bernasconi, S.M., Karson, J.A., Ludwing, K.A., Butterfield, D.A., et al., 2003. 30 000 years of hydrothermal activity at the Lost City vent field. Science 301, 495–498.
Fyfe, W.S., 1974. Heat of chemical reactions and submarine heat production. Geophysical Journal International 37, 213–315.
Gerlach, T.M., Taylor, B.E., 1990. Carbon isotope constraints on degassing of carbon-dioxide from Kilauea volcano. Geochimica et Cosmochimica Acta 54 (7), 2051–2058.
German, C.R., Higgs, N.C., Thomson, J., Mills, R., Elderfield, H., Blusztajn, J., et al., 1993. A geochemical study of metalliferous sediment from the TAG hydrothermal mound, 26°08'N. Mid-Atlantic Ridge Journal of Geophysical Research 98 (B6), 9683–9692.
German, C.E., Parson, L.M., Party, R.S., 1994. Charles Darwin cruise CD89, HEAT, hydrothermal exploration at the Azores Triple-Junction. Eos, Transactions, American Geophysical Union 75, 308.
German, C.R., Klinkhamme, G.P., Rudnicki, M., 1996a. The Rainbow hydrothermal plume, 36°15'N. MAR Geophysical Research Letters 23 (21), 2979–2982.
German, C.R., Parson, L.M., Team, H.S., 1996b. Hydrothermal exploration near the Azores Triple Junction: Tectonic control of venting at slow-spreading ridges? Earth and Planetary Science Letters 138, 93–104.
German, C.R., Colley, S., Palmer, M.R., Khripounoff, A., Klinkhammer, G.P., 2002. Hydrothermal plume-particle fluxes at 13°N on the East Pacific Rise. Deep-Sea Research Part I—Oceanographic Research Papers 49 (11), 1921–1940.
Gillis, K.M., Ludden, J.N., Smith, A.D., 1992. Mobilization of REE during crustal aging in the Troodos Ophiolite, Cyprus. Chemical Geology 98 (1–2), 71–86.
Gràcia, E., Charlou, J.-L., Radford-Knoery, J., Parson, L., 2000. Non-transform offset along the Mid-Atlantic ridge south of the Azores (38ºN–34ºN): Ultramafic exposures and hosting of hydrothermal vents. Earth and Planetary Science Letters 177, 89–103.
Hannington, M.D., Jonasson, I.R., Herzig, P.M., Peterson, S., 1995. Physical and chemical processes of seafloor mineralization at Mid-Ocean ridge. American Geophysical Union 115–157.
Hoefs, J., 1997. Stable Isotope Geochemistry. Springer-Verlag. 201 pp.
Holm, N.G., Charlou, J.L., 2001. Initial indications of abiotic formation of hydrocarbons in the Rainbow ultramafic hydrothermal system, Mid-Atlantic Ridge. Earth and Planetary Science Letters 191 (1–2), 1–8.
Janecky, D.R., Seyfried, W.E., 1986. Hydrothermal serpentinization of peridotite within the oceanic-crust: Experimental investigations of mineralogy and major element chemistry. Geochimica et Cosmochimica Acta 50 (7), 1357–1378.
Kelley, D.S., Karson, J.A., Blackman, D.K., Früh-Green, G.L., Butterfield, D.A., Lilley, M.D., et al., 2001. An off-axis hydrothermal vent field near the Mid-Atlantic Ridge at 30ºN. Nature 412, 445–449.
Kelley, D.S., Karson, J.A., Früh-Green, G.L., Yoerger, D.R., Shank, T.M., Butterfield, D.A., et al., 2005. A serpentinite-hosted ecosystem: The Lost City hydrothermal field. Science 307, 1428–1434.
Klinkhammer, C.P., Elderfield, H., Edmond, J.M., Mitra, A., 1994. Geochemical implications of rare earth element patterns in hydrothermal fluids from mid-ocean ridges. Geochimica et Cosmochimica Acta 58 (23), 5105–5113.
Krauskopf, K.B., 1957. Separation of manganese from iron in sedimentary processes. Geochimica et Cosmochimica Acta 12, 61–64.
Large, R.R., 1992. Australian volcanic-hosted massive sulfide deposits: Features, styles, and genetic models. Economic Geology and the Bulletin of the Society of Economic Geologists 87 (3), 471–510.
Lowell, R.P., Rona, P.A., 2002. Seafloor hydrothermal systems driven by the serpentinization of peridotite. Geophysical Research Letters 29 (11), 1–4.
Marques, A.F.A., Barriga, F., Scott, S.D., 2007. Sulfide mineralization in an ultramafic-rock hosted seafloor hydrothermal system: From serpentinization to the formation of Cu–Zn–(Co)-rich massive sulfides. Marine Geology 245, 20–39.
Mevel, C., 2003. Serpentinization of abyssal peridotites at mid-ocean ridges. Comptes Rendus Geosciences 335 (10–11), 825–852.
Michard, A., 1989. Rare earth element systematic in hydrothermal fluids. Geochimica et Cosmochimica Acta 53, 745–750.
Mills, R.A., Elderfield, H., 1995a. Hydrothermal activity and the geochemistry of metalliferous sediments. American Geophysical Union 91, 392–407.
Mills, R.A., Elderfield, H., 1995b. Rare earth element geochemistry of hydrothermal deposits from the active TAG Mound, 26ºN Mid-Atlantic Ridge. Geochimica et Cosmochimica Acta 95 (17), 3511–3524.
Mills, R., Elderfield, H., Thompson, J., 1993. A dual origin for the hydrothermal component in a metalliferous sediment core from the Mid-Atlantic Ridge. Journal of Geophysical Research 98 (B6), 9671–9682.

Miranda, J.M., Silva, P.F., Lourenço, N., Henry, B., Costa, R., Team, S., 2003. Study of the Saldanha massif (MAR, 36º34'N): Constrains from rock magnetic and geophysical data. Marine Geophysical Research 23, 299–318.
Moller, P., Morteani, G., Hoefs, J., Parekh, P.P., 1979. Origin of the ore-bearing solution in the Pb-Zn veins of the Western Harz, Germany, as deduced from rare-earth element and isotope distributions in calcites. Chemical Geology 26 (3–4), 197–215.
Moller, P., Morteani, G., Dulski, P., 1984. The origin of the calcites from Pb-Zn veins in the Harz Mountains, Federal Republic of Germany. Chemical Geology 45 (1–2), 91–112.
Moller, P., Luders, V., Schroder, J., Luck, J., 1991. Element partitioning in calcite as a function of solution flow-rate: A study on vein calcites from the Harz Mountains. Mineralium Deposita 26 (3), 175–179.
O'Brien, D., Carton, M., Eardly, D., Patching, J.W., 1998. In situ filtration and preliminary molecular analysis of microbial biomass from the Rainbow hydrothermal plume at 36°15'N on the Mid-Atlantic Ridge. Earth and Planetary Science Letters 157 (3–4), 223–231.
Ohmoto, H., 1986. Stable isotope geochemistry of ore deposits. In: Valley, J.W., Taylor, H.P., O'Neil, J.R. (Eds.), Stabe Isotopes in High Temperature Geological Processes. Reviews in Mineralogy and Geochemistry, pp. 491–559.
Ohmoto, H., Goldhaber, M.B., 1997. Sulfur and carbon isotopes. In: Barnes, H.L. (Ed.), Geochemistry of Hydrothermal Deposits. John Wiley & Sons, Inc, New York, pp. 517–611.
Parson, L., Grácia, E., Coller, D., German, C., Needham, H.D., 2000. Second-order segmentation; the relationship between volcanism and tectonism at the MAR, 38°N - 35°40′N. Earth and Planetary Science Letters 178, 231–251.
Paulick, H., Bach, W., Godard, M., De Hoog, J.C.M., Suhr, G., Harvey, J., 2006. Geochemistry of abyssal peridotites (Mid-Atlantic Ridge, 15°20'N, ODP Leg 209): Implications for fluid/rock interaction in slow spreading environments. Chemical Geology 234 (3–4), 179–210.
Perner, M., Kuever, J., Seifert, R., Pape, T., Koschinsky, A., Schmidt, K., et al., 2007. The influence of ultramafic rocks on microbial communities at the Logatchev hydrothermal field, located 15 degrees N on the Mid-Atlantic Ridge. Fems Microbiology Ecology 61 (1), 97–109.
Peter, J.M., Shanks, W.C., 1992. Sulfur, carbon, and oxygen isotope variations in submarine hydrothermal deposits of Guaymas Basin, Gulf of California, USA. Geochimica et Cosmochimica Acta 56 (5), 2025–2040.
Plank, T., Langmuir, C.H., 1998. The chemical composition of subducting sediment and its consequences for the crust and mantle. Chemical Geology 145 (3–4), 325–394.
Proskurowski, G., Lilley, M.D., Brown, T.A., 2004. Isotopic evidence of magmatism and seawater bicarbonate removal at the endeavour hydrothermal system. Earth and Planetary Science Letters 225 (1–2), 53–61.
Proskurowski, G., Lilley, M.D., Kelley, D.S., Olson, E.J., 2006. Low temperature volatile production at the Lost City Hydrothermal Field: Evidence from a hydrogen stable isotope geothermometer. Chemical Geology 229 (4), 331–343.
Proskurowski, G., Lilley, M.D., Seewald, J.S., Fruh-Green, G.L., Olson, E.J., Lupton, J.E., et al., 2008. Abiogenic hydrocarbon production at Lost City hydrothermal field. Science 319 (5863), 604–607.
Ribeiro da Costa I., 2005. Serpentinization on the Mid-Atlantic Ridge: The Rainbow, Saldanha and Menez Hom sites. PhD Thesis, Faculdade de Ciências da Universidade de Lisboa, Lisbon, 444 pp.
Schmidt, K., Koschinsky, A., Garbe-Schonberg, D., de Carvalho, L.M., Seifert, R., 2007. Geochemistry of hydrothermal fluids from the ultramafic-hosted Logatchev hydrothermal field, 15ºN on the Mid-Atlantic Ridge: Temporal and spatial investigation. Chemical Geology 242 (1–2), 1–21.
Schroeder, T., John, B., Frost, B.R., 2002. Geologic implications of seawater circulation through peridotite exposed at slow-spreading mid-ocean ridges. Geology 30, 367–370.
Seyfried, W.E., Dibble, W.E., 1980. Seawater-peridotite interaction at 300 °C and 500Bars: Implications for the origin of oceanic serpentinites. Geochimica et Cosmochimica Acta 44 (2), 309–321.
Seyfried, W.E., Berrndt, M.E., Seewald, J.S., 1988. Hydrothermal alteration processes at mid-ocean ridges: Constraints from diabase alteration experiments, hot-spring fluids and composition of the oceanic crust. Canadian Mineralogist 26, 787–804.
Seyfried Jr., W.E., Foustoukos, D.I., Fu, Q., 2007. Redox evolution and mass transfer during serpentinization: An experimental and theoretical study at 200 °C, 500 bar with implications for ultramafic-hosted hydrothermal systems at Mid-Ocean Ridges. Geochimica et Cosmochimica Acta 71 (15), 3872–3886.
Shanks III, W.C., Böhlke, J.K., Seal II, P.R., 1995. Stable isotopes in midocean ridge hydrothermal systems: Interactions between fluids, minerals, and organisms. In: Humphris, S.E., Zierenberg, R.A., Mullineaux, L.S., Thompson, R.E. (Eds.), Seafloor Hydrothermal Systems: Physical, Chemical, Biological, and Geological Interactions. American Geophysical Union, Geophysical Monography, pp. 194–221.
Sinha, M., Dzhatieva, Z., Santos, F., Silva, N., Dias, A., Marques, A., et al., 2005. Active electromagnetic survey of hydrothermal venting area at Saldanha Massif, Mid-Atlantic Ridge. Geophysical Research Abstracts 7 EGU05-A-07706.
Sinha, M.C., Dzhatieva, Z., Dias, A., Fredrichs, N., 2006. RRS Charles Darwin Cruise 167, 23 Nov–21 Dec 2004. Sub-seafloor physical properties at Saldanha Seamount, Mid-Atlantic Ridge, and controls on the spatial distribution of hydrothermal venting. National Oceanography Centre Southampton, Southampton, UK.
Smith, D.K., Cann, J.R., Escartin, J., 2006. Widespread active detachment faulting and core complex formation near 13° N on the Mid-Atlantic Ridge. Nature 442 (7101), 440–443.
Spangenberg, J., Fontbote, L., Sharp, Z.D., Hunziker, J., 1996. Carbon and oxygen isotope study of hydrothermal carbonates in the zinc-lead deposits of the San Vicente district, central Peru: A quantitative modeling on mixing processes and CO2 degassing. Chemical Geology 133 (1–4), 289–315.
Stakes, D.S., Oneil, J.R., 1982. Mineralogy and Stable Isotope Geochemistry of Hydrothermally Altered Oceanic Rocks. Earth and Planetary Science Letters 57 (2), 285–304.
Sverjensky, D.A., 1984. Europium redox equilibria in aqueous solution. Earth and Planetary Science Letters 67 (1), 70–78.
Taylor, B.E., 1986. Magmatic volatiles; isotopic variation of C, H, and S. In: Valley, J.W., Taylor, H.P., O'Neil, J.R. (Eds.), Stable Isotopes in High temperature Geological Processes. Reviews in Mineralogy and Geochemistry, pp. 185–225.
Taylor, S.R., McLennan, S.M., 1985. The Continental Crust: its Composition and Evolution: An Examination of the Geochemical Record Preserved in Sedimentary Rocks. Blackwell Science Inc, Oxford.
Van der Flier-Keller, E., 1991. Geochemistry and mineralogy of sediments, Atlantis II fracture zone, southwest Indian Ocean. Proceedings of the Ocean Drilling Project, Scientific Results 118, 145–151.
Vaughan, D.J., Craig, J.R., 1986. Sulphide ore minerals stabilities, morphologies, and intergrowth textures. In: Barnes, H.L. (Ed.), Geochemistry of Hydrothermal Ore Deposits. John Wiley & Sons, New York, pp. 367–486.
Welhan, J.A., Lupton, J.E., 1987. Light-Hydrocarbon Gases in Guaymas Basin Hydrothermal Fluids: Thermogenic Versus Abiogenic Origin. Aapg Bulletin-American Association of Petroleum Geologists 71 (2), 215–223.
Wetzel, L.R., Shock, E.L., 2000. Distinguishing ultramafic from basalt-hosted submarine hydrothermal systems by comparing calculated vent fluid compositions. Journal of Geophysical Research-Solid Earth 105 (B4), 8319–8340.
Wildeman, T.R., Haskin, L.A., 1965. Rare-earth elements in ocean sediments. Journal of Geophysical Research 70 (12), 2905–2910.
Zheng, Y.F., 1990. Carbone-oxigen isotopic covariation in hydrothermal calcite during degassing of CO2: A quantitative evaluation and application to the Kushikino gold mining area in Japan. Mineralium Deposita 25 (4), 246–250.
Zheng, Y.F., Hoefs, J., 1993. Carbon and oxygen isotopic covariations in hydrothermal calcites: Theoretical modeling on mixing processes and application to Pb-Zn deposits in the Harz Mountains, Germany. Mineralium Deposita 28 (2), 79–89.